

Article

Microstructure and Fracture Toughness of Nitrided D2 Steels Using Potential-Controlled Nitriding

Ki-Hong Kim ¹, Won-Beom Lee ¹, Tae-Hwan Kim ^{1,2} and Seok-Won Son ^{1,2,*}

¹ Heat & Surface Technology R&D Department, Research Institute of Advanced Manufacturing & Materials Technology (KITECH), Siheung 15014, Korea; khkim9340@gmail.com (K.-H.K.); wbeom70@kitech.re.kr (W.-B.L.); hwan2@kitech.re.kr (T.-H.K.)

² Department of Materials Science and Engineering, Inha University, Incheon 22212, Korea

* Correspondence: ssw214@kitech.re.kr; Tel.: +82-31-8084-8654

Abstract: Potential-controlled nitriding is an effective technique for enhancing the life of steel molds and dies by improving their surface hardness and toughness against fatigue damage. In this study, the effect of the nitriding potential on the microstructure and fracture toughness of nitrided AISI D2 steels was investigated. The nitrided layers were characterized by microhardness measurements, optical microscopy, and scanning electron microscopy, and their phases were identified by X-ray and electron backscatter diffraction. As the nitriding potential increased to 2.0 atm^{-1/2}, an increase in the surface hardness and fracture toughness was observed with the growth of the compound layer. However, both the surface hardness and the fracture toughness decreased at the higher nitriding potential of 5.0 atm^{-1/2} owing to the increased porosity in the compound layers, which mainly consist of the ϵ (Fe₂₋₃N) phase. Additionally, by observing crack growth behavior, the fracture toughness was analyzed considering the material characteristics of the diffusion and compound layers. The fracture toughness was influenced by the location of the initial Palmqvist cracks due to the localized plastic deformation of the diffusion layer and increased crack length due to the porous compound layer.



Citation: Kim, K.-H.; Lee, W.-B.; Kim, T.-H.; Son, S.-W. Microstructure and Fracture Toughness of Nitrided D2 Steels Using Potential-Controlled Nitriding. *Metals* **2022**, *12*, 139. <https://doi.org/10.3390/met12010139>

Academic Editors: Filippo Berto, Ricardo Branco and Yanxin Qiao

Received: 18 December 2021

Accepted: 6 January 2022

Published: 11 January 2022

Publisher's Note: MDPI stays neutral with regard to jurisdictional claims in published maps and institutional affiliations.



Copyright: © 2022 by the authors. Licensee MDPI, Basel, Switzerland. This article is an open access article distributed under the terms and conditions of the Creative Commons Attribution (CC BY) license (<https://creativecommons.org/licenses/by/4.0/>).

Keywords: nitride materials; X-ray diffraction; diffusion; precipitation

1. Introduction

High-carbon, high-chromium AISI D2 steel, also known as cold work tool steel, is widely used in the fabrication of punches, shear knives, tools, molds, and dies because of its hardenability and high resistance to wear and softening [1,2]. Recently, it has been utilized for various manufacturing applications to enhance the working life of components against impact, shear, and fatigue damage [3–5]. For instance, cold work tool steel performance was improved by modifying its chemical composition to obtain high strength, toughness, and high fatigue resistance [3]. Heat treatment processes, such as cryogenic treatment and salt bath quenching, were also developed to further improve the hardness, toughness, and wear resistance of cold work tool steel [4,5].

Well-known techniques for surface modification, such as nitriding treatment (e.g., compound-free, ion-nitriding) and physical vapor deposition (e.g., TiN, AlTiN coatings), have been studied and implemented to improve the working performance of molds and dies [6–8]. Nitriding is one of the most useful thermochemical surface treatments because it can be performed at temperatures of 450–600 °C, resulting in low distortion and high surface hardness [9,10]. However, there are deleterious effects on the mechanical properties of the nitrided layers, namely decreased surface hardness, wear resistance, and toughness [8,11]. This is due to the presence of excess nitrogen and discontinuous precipitation, which result in the coarsening of the nitrides and porosity of the compound layer during nitriding [12]. Techniques such as ion-nitriding and gas-controlled nitriding have been developed to guarantee the long service life of the nitrided layer [13–15].

Mechanical properties, such as high surface hardness and wear resistance, combined with toughness, are required to enhance the durability of steel dies and molds [16,17]. As reported by Yong et al. [18], the low toughness of the compound layer leads to brittle cracks and decreases the die and mold thickness owing to wear damage, resulting in the cracking and spalling of the compound layer. Nolan et al. [19] applied plasma nitrided treatment on AISI H11 steel to evaluate the fracture toughness of the compound layers as a function of indentation load using the Vickers hardness test and established that fracture toughness is dependent on the compound layer thickness owing to different crack behaviors. The elastic and toughness properties of the nitrided layers were recently investigated using micro-mechanical tensile test methods [20]. To improve the life of die and mold steel, a controlled nitriding process that involves regulating the applied nitriding potential K_n is crucial for minimizing the crack growth of the nitrided layer [21].

As mentioned earlier, the fracture toughness of nitrided AISI D2 steel relies heavily on the material characteristics of the nitrided layers. In other words, the thickness of the compound layer, as well as the phase evolution of the nitrided layer, must be evaluated in order to accurately estimate the fracture behavior, which can be achieved by controlling the nitriding potential [22]. However, studies on this topic using die and mold steels are scarce. Herein, we investigated the effect of the nitriding potential on the microstructural evolution and fracture toughness of nitrided AISI D2 steel. This steel was chosen as it is widely applied in the gas nitriding process to prolong die and mold working life. The crack growth behavior of the nitrided layers is analyzed in detail to verify its association with fracture toughness.

2. Materials and Methods

The chemical composition of the AISI D2 steel used is listed in Table 1. Specimens of size $\text{Ø}30 \text{ mm} \times 10 \text{ mm}$ were prepared and subjected to the following heat treatment procedure to obtain a hardness of approximately 56 HRC. The specimens were austenitized at 1035 °C in a vacuum furnace, quenched in N_2 gas at 3 bar pressure, and double-tempered for 90 min at different temperatures of 550 and 560 °C . Prior to the gaseous nitriding process, the quenched and tempered (QT) AISI D2 specimens were ground to 1500 grits using several grades of SiC sandpaper and cleaned with ethanol in an ultrasonicator bath. Gas nitriding was then performed in a nitriding furnace (SECO/WARWICK, HRNe606090), as illustrated schematically in Figure 1. Pre-heating was conducted at 350 °C ; this was followed by gas nitriding in NH_3 gas at 520 °C for 10 h. The gas atmosphere during nitriding was controlled using a hydrogen sensor.

Table 1. Chemical composition of AISI D2 steel (wt.%).

C	Si	Mn	P	S	Cr	Mo	V	Fe
1.52	0.4	0.53	0.04	0.02	12.8	0.99	0.38	Bal.

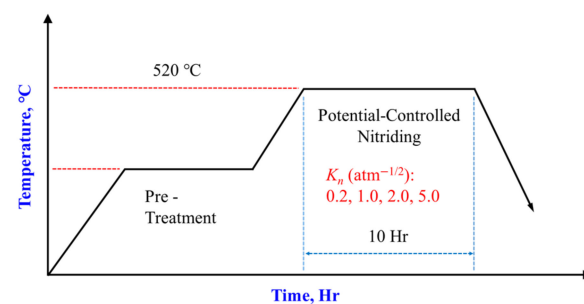


Figure 1. Nitriding of AISI D2 specimens as a function of nitriding potential.

Then, the nitriding potential K_n , which defines the chemical potential of nitrogen related to the evolution of the nitrided layer, was calculated using the H_2 gas fraction. To investigate the effect of nitriding potential, the nitriding potentials were kept stable

at 0.2, 1.0, 2.0, and 5.0 atm^{-1/2} for each nitriding process as per AMS 2759-10B. The nitriding process can be expressed by the decomposition reactions of nitrogen from NH₃ gas as follows:



$$K_n = \frac{P_{\text{NH}_3}}{P_{\text{H}_2}^{3/2}} \quad (2)$$

where P_{NH_3} is the partial pressure of ammonia, and P_{H_2} is that of hydrogen. After the nitriding treatment, the surface and section hardnesses were obtained using a Vickers micro-hardness tester (Future Tech, FLV-10 ARS-F, Kawasaki, Japan) with a load of 100 gf for a dwell time of 10 s. At least five measurements at each section were taken, and the average hardness value was obtained. The effective hardening depth was determined as the depth corresponding to the high 50 HV_{0.1} from the hardness of the quenched and tempered specimen as per ISO 18203.

To characterize the microstructure, the nitrided specimens were etched with a mixture of 100 mL ethanol and 3% nitric acid solution. The cross-sectional microstructures were then observed using optical microscopy and scanning electron microscopy (SEM, FEI, NNS450, Hillsboro, OR, USA). To determine the phase evolution of the nitrided specimens, X-ray diffraction (XRD, PANalytical, X'Pert-PRO MPD, Malvern, UK) was performed under accelerating conditions of 40 kV and 30 mA and diffraction angle measurements from 20° to 90° using the Cu-Kα target were taken. Electron backscatter diffraction (EBSD, Hitachi, SU5000, Tokyo, Japan) was performed to characterize the phase of the compound layer. Finally, hardness measurements were carried out using a Vickers macrohardness tester (Mitutoyo HV-100, 810–440 K, Kawasaki, Japan) with a load of 50 kgf for a dwell time of 5 s, and the Vickers hardness (HV) was calculated using Equation (3) [23]:

$$HV = 1.8544P/d_m^2 \quad (3)$$

where P is the indentation load (kgf), and d_m is the mean indentation diagonal (mm). To determine the fracture toughness of the nitrided layer, the Palmqvist-method was used by estimating the total crack length. The Palmqvist crack lengths at the indentation corners were measured using SEM at 500× magnification. The fracture toughness was calculated using Equation (4) [23]:

$$K_{Ic} = 0.0028 \cdot HV^{1/2} \cdot \left(\frac{P}{T}\right)^{1/2} \quad (4)$$

where T is the total crack length (mm).

3. Results

3.1. Hardness

Figure 2 shows the hardness profiles of the QT material and nitrided specimens in relation to the distance from the surface. The average hardness of the heat-treated specimen was 570 HV_{0.1}. With a nitriding potential of $K_n = 0.2$ atm^{-1/2}, the hardness was approximately 1130 HV_{0.1} on the surface of the nitrided layer, which decreased as the depth increased. The case depth at $K_n = 0.2$ atm^{-1/2} was measured to be approximately 100 μm from the top surface. With a nitriding potential of $K_n = 1.0$ atm^{-1/2}, the surface hardness and the case depth increased to about 1260 HV_{0.1} and 130 μm, respectively. As K_n increased to 2.0 atm^{-1/2}, the surface hardness reached a maximum value of approximately 1270 HV_{0.1}, and there was no significant change in the case depth with the increase in nitriding potential. However, at $K_n = 5.0$ atm^{-1/2}, the decrease in surface hardness was observed to be approximately 960 HV_{0.1}. The compound layer grew with the increase of the nitriding potential to 2.0 atm^{-1/2}. However, the hardness profile at $K_n = 5.0$ atm^{-1/2} deviated from the general shape.

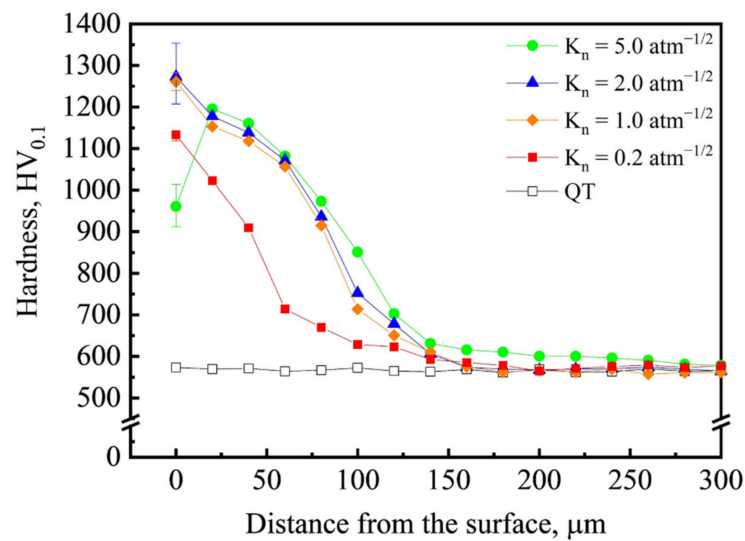


Figure 2. Hardness profiles of the QT and nitrided specimens as a function of distance from the top surface.

3.2. Microstructure

The cross-sectional microstructures of the QT and nitrided AISI D2 specimens are shown in Figure 3. In the QT base material, primary carbides were observed in tempered martensite owing to quenching and tempering. With a nitriding potential of $K_n = 0.2 \text{ atm}^{-1/2}$, the compound layer was finely formed till about $0.7 \mu\text{m}$ from the top surface (Figure 3a). In particular, at the nitriding potential of $K_n = 1.0 \text{ atm}^{-1/2}$, the compound layer grew to about $2 \mu\text{m}$, and chromium nitrides (CrN) were distinctly observed in the diffusion layer (Figure 3b). With increasing nitriding potentials ($K_n = 2.0 \text{ atm}^{-1/2}$ to $K_n = 5.0 \text{ atm}^{-1/2}$), the compound layer remarkably grew from about $7.8 \mu\text{m}$ to $8.7 \mu\text{m}$ (Figure 3c,d, respectively).

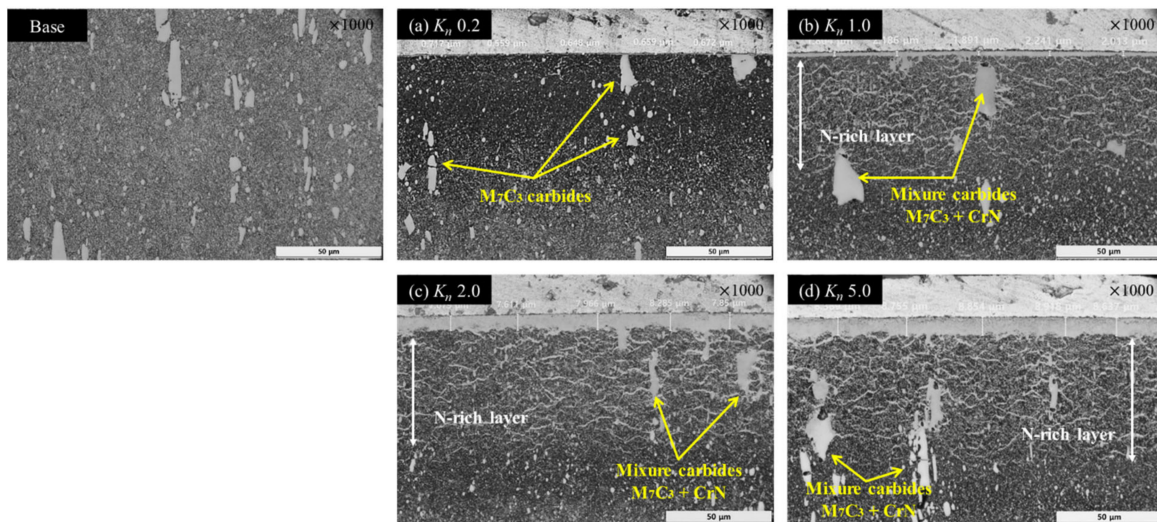


Figure 3. Cross-sectional microstructures of the nitrided specimens after nitriding at $520 \text{ }^\circ\text{C}$ for 10 h at $K_n =$ (a) 0.2, (b) 1.0, (c) 2.0, and (d) $5.0 \text{ atm}^{-1/2}$.

Figure 4 shows the XRD patterns of the QT and nitrided AISI D2 specimens. Diffraction peaks of iron ($\alpha\text{-Fe}$), cementite (M_3C), and carbide (M_7C_3) were detected on the surface of the QT base material. With a nitriding potential of $K_n = 0.2 \text{ atm}^{-1/2}$, nitride peaks corresponding to chromium nitrides (CrN), γ' (Fe_4N), and ϵ (Fe_{2-3}N) phases were weakly observed on the surface of the nitrided layer. With an increase in the nitriding potential ($K_n = 1.0\text{--}5.0 \text{ atm}^{-1/2}$), ϵ (Fe_{2-3}N) peaks were mainly observed on the surface of the nitrided specimens.

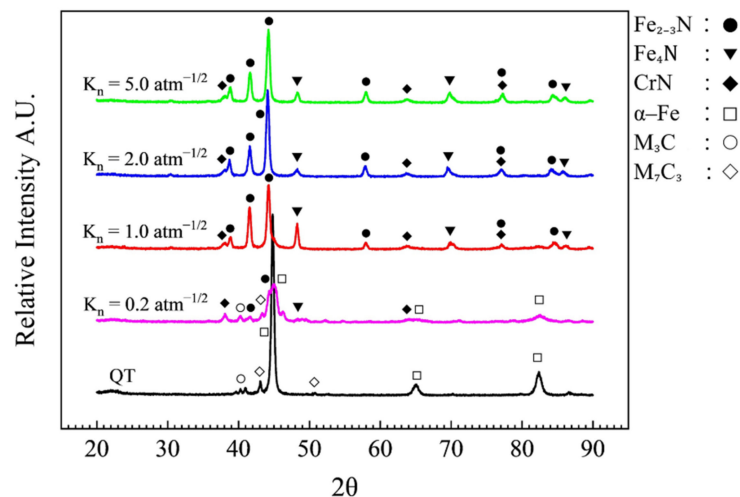


Figure 4. X-ray diffraction pattern of the QT and nitrided specimens.

Figure 5 shows the EBSD of the nitrided AISI D2 specimens for characterizing the phase of the nitrided layers. Prior to phase analysis, the phases of the compound layer can be easily distinguished to consist of ϵ (Fe₂₋₃N) and γ' (Fe₄N) phases, which have hexagonal close-packed (HCP) and face-centered cubic (FCC) structures, respectively [24]. At the lower nitriding potential (0.2 atm^{-1/2}), the α -Fe phase was detected on the surface of the nitrided layer, and there were no obvious nitride phases consisting of ϵ (Fe₂₋₃N) and γ' (Fe₄N) near the nitrided surface. At $K_n = 1.0$ atm^{-1/2}, the ϵ (Fe₂₋₃N) phase, which consisted of the compound layer, was mainly observed, and the γ' (Fe₄N) phase was finely detected around the compound layer. As the nitriding potential increased from 2.0 to 5.0 atm^{-1/2}, the compound layer, which mainly consisted of the ϵ (Fe₂₋₃N) phase, grew remarkably on the surface of the nitrided AISI D2 specimens. From both XRD and EBSD phase analyses, it was found that the compound layer of the nitrided AISI D2 specimens mainly consisted of the ϵ (Fe₂₋₃N) phase.

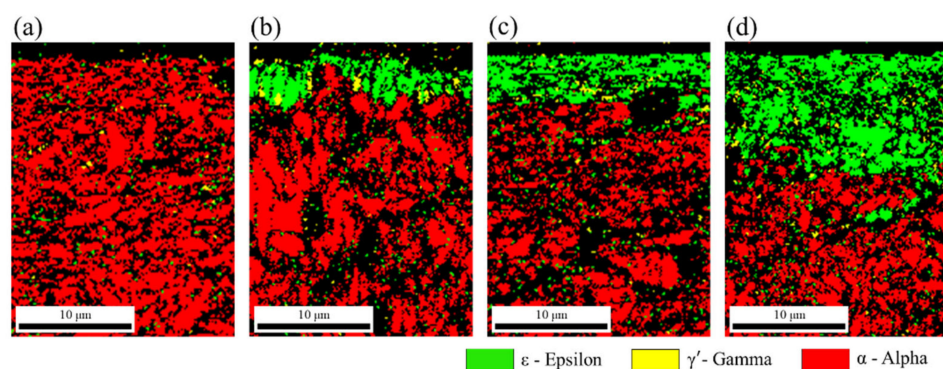


Figure 5. EBSD phase maps analyzed near the compound layer of the nitrided specimens after nitriding at 520 °C for 10 h at $K_n =$ (a) 0.2, (b) 1.0, (c) 2.0, and (d) 5.0 atm^{-1/2}.

3.3. Fracture Toughness

Figure 6 shows the fracture toughness (K_{Ic}) as a function of various nitriding potentials compared with the surface hardness and compound layer thickness. With a nitriding potential of $K_n = 0.2$ atm^{-1/2} and a compound layer of 0.7 μm thickness, the fracture toughness and the surface hardness were observed to be about 8.5 MN/m^{3/2} and 1130 HV_{0.1}, respectively. As the nitriding potential increased to 2.0 atm^{-1/2}, the compound layer thickness increased, and the maximum fracture toughness and surface hardness were measured to be approximately 12.6 MN/m^{3/2} and 1270 HV_{0.1}, respectively. However, at the higher nitriding potential of $K_n = 5.0$ atm^{-1/2}, the fracture toughness decreased to approximately 10.0 MN/m^{3/2} with the decrease in the surface hardness despite the compound layer

thickness increasing to 8.7 μm . Thus, the fracture toughness was found to be related to surface hardness.

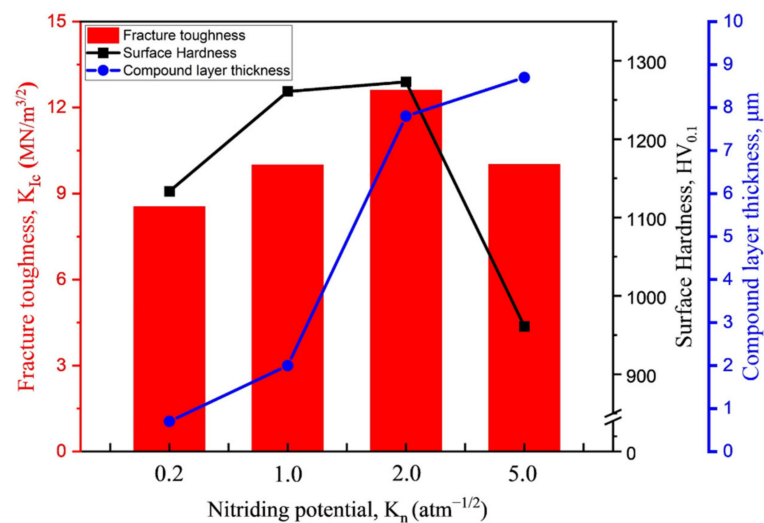


Figure 6. Fracture toughness of the nitrided AISI D2 specimens compared with the surface hardness and compound layer thickness as a function of the nitriding potentials.

3.4. Crack Characteristics

To examine the effect of the nitriding potential on the fracture toughness with the evolution of the nitrided layer, the crack characteristics were investigated through Vickers indentation. Figure 7 shows SEM images of the Palmqvist cracks and ring-shaped cracks. With the increase in nitriding potential ($K_n = 0.2$ to $K_n = 2.0$ $\text{atm}^{-1/2}$), the Palmqvist crack length gradually decreased to 45 μm with the growth of the compound layer. However, at $K_n = 5.0$ $\text{atm}^{-1/2}$, the crack length increased again to approximately 70.4 μm , despite the growth of the compound layer to approximately 8.7 μm . In addition, around the indentation edges, the length of the ring-shaped cracks decreased with the growth of the compound layer as K_n increased from 0.2 to 2.0 $\text{atm}^{-1/2}$, which became zero (no ring-shaped cracks) at $K_n = 5.0$ $\text{atm}^{-1/2}$.

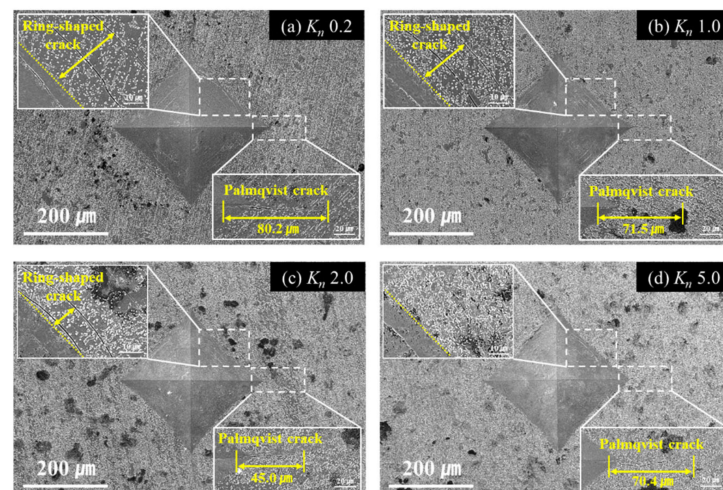


Figure 7. SEM images of the nitrided surface showing the ring-shaped cracks and Palmqvist cracks due to the Vickers indentation under various nitriding potentials at $K_n =$ (a) 0.2, (b) 1.0, (c) 2.0, and (d) 5.0 $\text{atm}^{-1/2}$.

Figure 8 shows the crack patterns occurring in the compound-free nitrided layer, obtained by polishing the compound layer on the nitrided surface ($K_n = 0.2$ $\text{atm}^{-1/2}$). As observed in Figure 8a, the ring-shaped cracks occurred around the indented area due to

the plastic deformation in the compound-free nitrified layer, and semi-circular cracks were formed beneath the indentation. As shown in Figure 8b, micro-cracks were formed along the primary carbides when the Palmqvist crack propagated outward along the diagonal of the indentation.

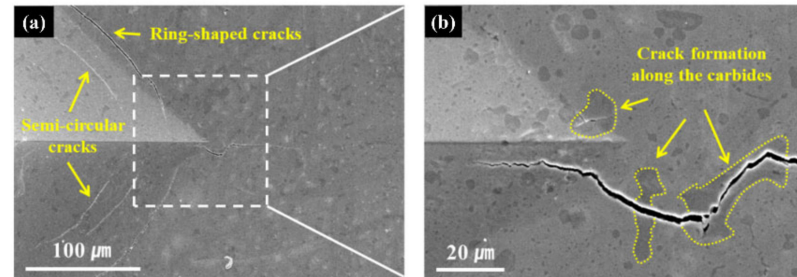


Figure 8. SEM images of the nitrified surface (compound-free) showing (a) semi-circular cracks and (b) crack formation along the coarse carbides.

4. Discussion

In this study, we investigated the effect of the nitriding potential on the evolution of the nitrified layers, and consequently, the fracture toughness by analyzing the crack propagation. The results indicate that the nitriding potential has a significant effect on fracture toughness. In addition, a previous study [19] showed that the fracture toughness is dependent on the thickness of the compound layer; however, in this study, it was verified that phases, such as the chromium nitrides (CrN) and iron nitrides (ϵ -Fe₂₋₃N), and the porous compound layer significantly influenced the different behaviors of crack growth that resulted from the indentation. It was found that these were the main factors affecting fracture toughness and surface hardness.

As shown by the SEM images in Figure 9a–f, with increasing nitriding potential ($K_n = 0.2$ – $5.0 \text{ atm}^{-1/2}$), the initial Palmqvist crack moves nearer to the indentation corners with the growth of compound layers. At the lower nitriding potential ($0.2 \text{ atm}^{-1/2}$), the semi-circular cracks were formed beneath the Vickers indentation (see Figure 9a). Subhash et al. [25] reported that micro-cracks are developed by localized plastic deformation (shear bands) owing to the Vickers indentation, which then grows into semi-circular cracks. The crack characteristics of nitrified H11 steel are dependent on the thickness of the compound layer, as reported by Nolan et al. [19].

For the crack characteristics of the nitrified mold steel, alloy compositions (Cr, Mo, V, etc.) affect the precipitation reactions of the diffusion layer. During the nitriding process, M_7C_3 gradually decomposes with decarburization as CrN grows. In this recrystallization, the M_7C_3 retains discontinuous morphologies of carbide [26–28]. In particular, as shown in Figure 10, a discontinuous precipitation network of newly formed carbides (M_xC_y) is present in the carbon-rich zone along the coarse CrN nitrides. As the localized plastic deformation occurred during the Vickers indentation, the interface brittle cracks, as shown in Figure 8, developed at the weakly bonded interfaces between the different precipitates. This crack formation during the localized plastic deformation of the diffusion layer was found to be influenced by the initial Palmqvist cracks. Accordingly, at the lower nitriding potential ($K_n = 0.2 \text{ atm}^{-1/2}$), the fracture toughness was the lowest at $8.5 \text{ MN/m}^{3/2}$ when the crack length was 80.2 μm .

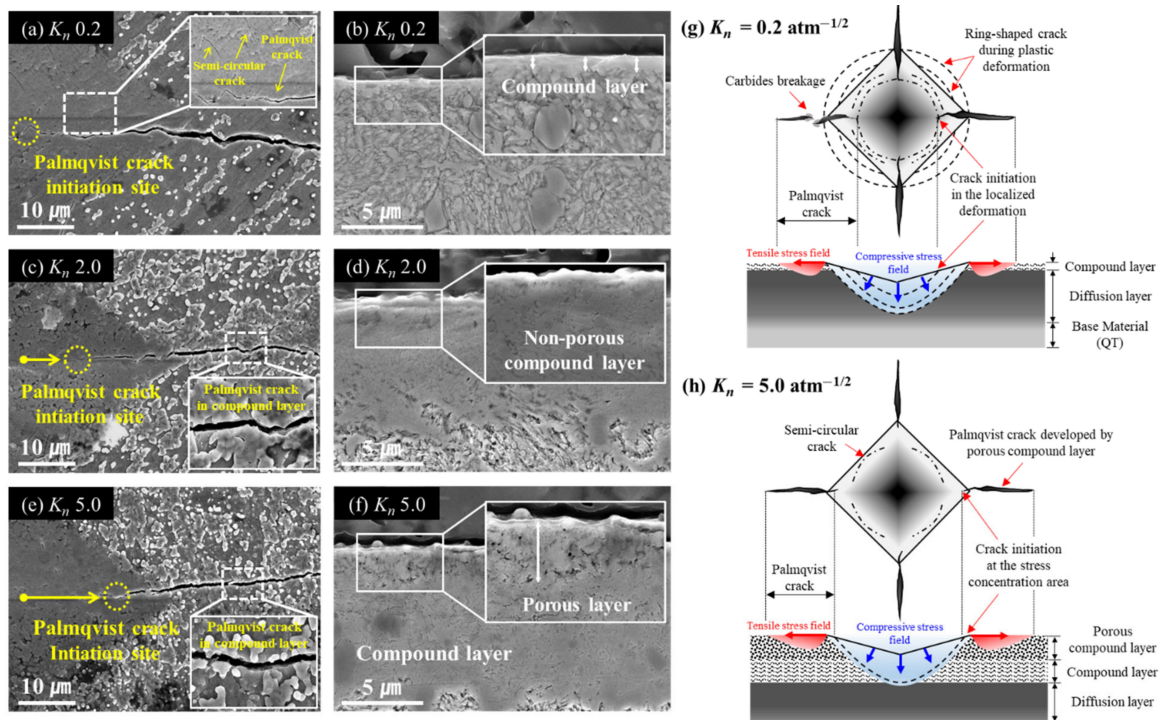


Figure 9. SEM images showing the locations of initial Palmqvist cracks on the nitrided surface (a,c,e) corresponding to the cross-sectional microstructures of compound layers (b,d,f), and schematic diagrams of crack patterns near the nitrided surface showing the different crack growth behaviors at $K_n =$ (g) 0.2, and (h) 5.0 $\text{atm}^{-1/2}$.

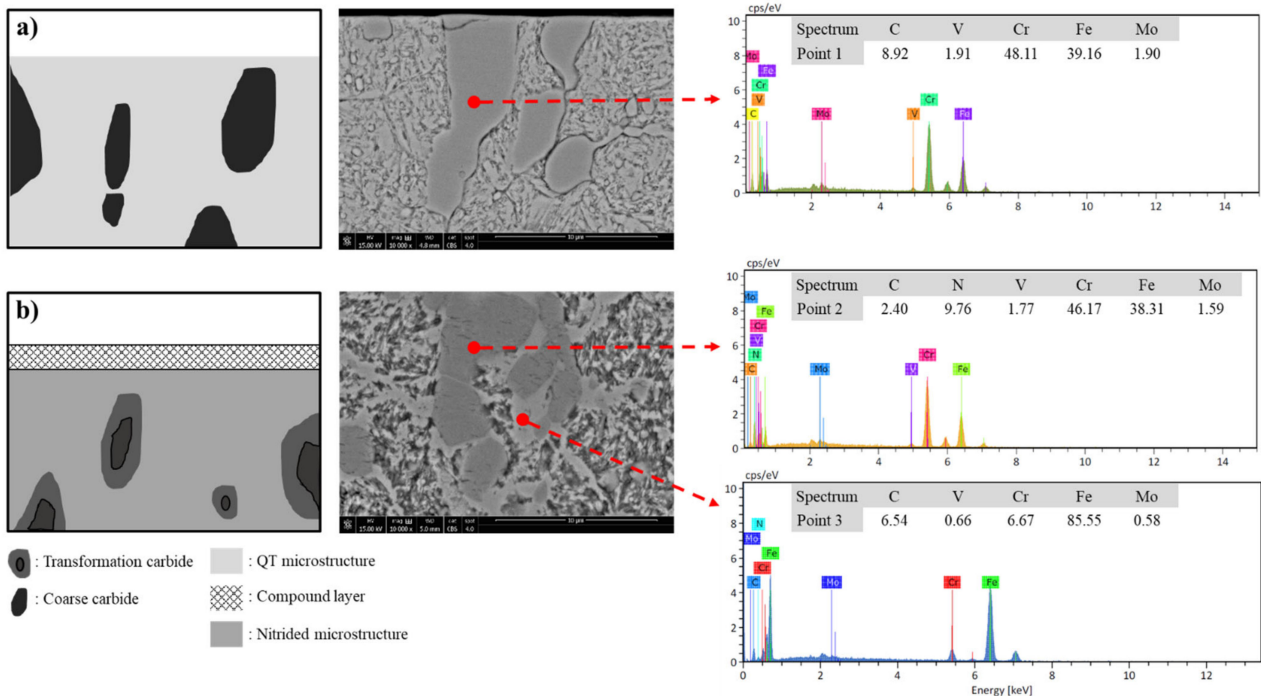


Figure 10. Schematic drawings of cross-sectional surface and SEM-EDX analysis showing (a) the base material (QT) and (b) nitrided D2 steel.

As shown in Figure 9a–f, with increasing nitriding potential ($K_n = 0.2\text{--}5.0 \text{ atm}^{-1/2}$), the initial Palmqvist cracks move closer to the indentation corners with the growth of compound layers. This eventually leads to a decrease in the length of the Palmqvist crack to approximately 45.5 μm owing to the differently located initial cracks (see Figures 7c and 9c).

Therefore, at the nitriding potential of $2.0 \text{ atm}^{-1/2}$, the fracture toughness was found to be the highest at approximately $12.6 \text{ MN/m}^{3/2}$. However, at the higher nitriding potential of $5.0 \text{ atm}^{-1/2}$, the crack length increased again to approximately $70.4 \mu\text{m}$ as the compound layer grew to approximately $8.7 \mu\text{m}$ (Figure 7d). This may be related to the porous layer formed near the surface of the compound layer (Figure 9f) due to the weakly bonded dissolved nitrogen at the higher nitriding potential [29,30]. These porosities near the surface of the compound layer led to a decrease in the surface hardness owing to stress concentrations during the Vickers indentation. Thus, the increase in the Palmqvist crack length was influenced by the porosity of the compound layer, and thereby, the consequent fracture toughness decreased to approximately $10.0 \text{ MN/m}^{3/2}$.

In the diffusion layers developed by the nitriding potential, the discontinuous precipitation network of the carbides (M_xC_y) grew in the carbon-rich zone along the coarse CrN nitrides. Furthermore, at a higher nitriding potential, the compound layer consisting of the ϵ (Fe_{2-3}N) phase grew and developed pores near the surface of the compound layer due to excess nitrogen. These material characteristics are closely related to surface hardness and fracture toughness. Thus, the crack growth behavior can be briefly described by a schematic diagram (Figure 9g,h) of the crack patterns in the nitrided AISI D2 specimens. This figure shows the location of initial cracks according to the localized plastic deformation in the diffusion layer and the increase in the crack length due to the porous compound layer. With the low nitriding potential of $K_n = 0.2 \text{ atm}^{-1/2}$, the ring-shaped cracks grew radially out toward the indentation due to the plastic deformation of the diffusion layers and inside the indentation; micro-cracks grew and developed into Palmqvist cracks due to the interface of the weakly bonded precipitates. Therefore, the fracture toughness was the lowest at the nitriding potential of $0.2 \text{ atm}^{-1/2}$. However, at $K_n = 5.0 \text{ atm}^{-1/2}$, the porosities developed on the surface of the compound layer led to an increase in the crack length (Figure 9h). Thus, the control nitriding for D2 steel can be effectively used to form the non-porous compound layer, which leads to the increase in fracture toughness by controlling the K_n .

5. Conclusions

In this study, the evolution of nitrided layers and fracture toughness of AISI D2 steels were investigated using various nitriding potentials.

- The average hardness of the heat-treated specimen was measured to be $570 \text{ HV}_{0.1}$, whereas that of the nitrided steel peaked at $1270 \text{ HV}_{0.1}$ for applied nitriding potentials below $5.0 \text{ atm}^{-1/2}$. At the high nitriding potential of $K_n = 5.0 \text{ atm}^{-1/2}$, the surface hardness decreased to about $960 \text{ HV}_{0.1}$.
- Chromium nitrides (CrN) develop in the diffusion layer as the carbide precipitation network grows in the carbon-rich zone owing to the recrystallization resulting from nitrogen diffusion. At a nitriding potential of $5.0 \text{ atm}^{-1/2}$, a compound layer consisting of the ϵ (Fe_{2-3}N) phase grows and develops pores near the surface of the compound layers due to the excess nitrogen.
- The fracture toughness was measured to be approximately $8.5 \text{ MN/m}^{3/2}$ at $K_n = 0.2 \text{ atm}^{-1/2}$ at which the compound layer had a thickness of about $0.7 \mu\text{m}$. As K_n was increased to $2.0 \text{ atm}^{-1/2}$, the compound layer further increased in thickness, and the fracture toughness peaked at $12.6 \text{ MN/m}^{3/2}$. However, as K_n was further increased to $5.0 \text{ atm}^{-1/2}$, the fracture toughness decreased to approximately $10.0 \text{ MN/m}^{3/2}$ with a decrease in the surface hardness, despite the compound layer growing up to $8.7 \mu\text{m}$ thick. Thus, the fracture toughness was found to be related to the surface hardness.
- Two main reasons for different crack growth behaviors of the nitrided layers with changes in the nitriding potentials were observed: the location of the initial crack inside the indentation due to the localized deformation of the diffusion layer and an increased crack length due to the porous compound layer. These main factors affected the fracture toughness. In short, with the growth of the non-porous compound layer, the increase in fracture toughness was closely related to the location of the initial crack.

This study showed that potential-controlled nitriding can be extended to molds and dies and can improve their mechanical properties, prolonging their service lives.

Author Contributions: Writing—original draft, K.-H.K.; manuscript review and editing, S.-W.S. and K.-H.K.; methodology, W.-B.L. and S.-W.S.; data curation, K.-H.K.; Formal analysis, S.-W.S. and K.-H.K.; visualization, K.-H.K.; investigation, S.-W.S. and T.-H.K.; resources, S.-W.S. and T.-H.K.; supervision, W.-B.L.; funding acquisition, W.-B.L. All authors have read and agreed to the published version of the manuscript.

Funding: This research received no external funding.

Institutional Review Board Statement: Not applicable.

Informed Consent Statement: Not applicable.

Data Availability Statement: The data are available from the authors upon reasonable request.

Acknowledgments: This work was supported by the Material parts technology development project (program: 20012857) funded by the Ministry of Trade, industry & Energy (MI, Korea).

Conflicts of Interest: The authors declare no conflict of interest.

References

1. Roberts, G.; Krause, G.; Kennedy, R. *Tool Steels*, 5th ed.; ASM International: Materials Park, OH, USA, 1998; pp. 203–217.
2. Bombac, D.; Fazarinc, M.; Saha Podder, A.; Kugler, G. Study of carbide evolution during thermo-mechanical processing of AISI D2 tool steel. *J. Mater. Eng. Perform.* **2013**, *22*, 742–747. [[CrossRef](#)]
3. Fukaura, K.; Yokoyama, Y.; Yokoi, D.; Tsujii, N.; Ono, K. Fatigue of cold-work tool steels: Effect of heat treatment and carbide morphology on fatigue crack formation, life, and fracture surface observations. *Metall. Mater. Trans. A* **2004**, *35*, 1289–1300. [[CrossRef](#)]
4. Das, D.; Dutta, A.K.; Ray, K.K. Influence of varied cryotreatment on the wear behavior of AISI D2 steel. *Wear* **2009**, *266*, 297–309. [[CrossRef](#)]
5. Torkamani, H.; Raygan, S.; Rassizadehghani, J. Comparing microstructure and mechanical properties of AISI D2 steel after bright hardening and oil quenching. *Mater. Des.* **2014**, *54*, 1049–1055. [[CrossRef](#)]
6. Unterweiser, P.M.; Gray, A.G. *Source Book on Nitriding*; ASM International: Metals Park, OH, USA, 1977; pp. 1–25.
7. Podgornik, B.; Sedlacek, M.; Cekada, M.; Jacobson, S.; Zajec, B. Impact of fracture toughness on surface properties of PVD coated cold work tool steel. *Surf. Coat. Technol.* **2015**, *277*, 144–150. [[CrossRef](#)]
8. Diaz-Guillen, J.C.; Naeem, M.; Hdz-Garcia, H.M.; Acevedo-Davila, J.L.; Diaz-Guillen, M.R.; Khan, M.A.; Iqbal, J.; Mtz-Enriquez, A.I. Duplex plasma treatment of AISI D2 tool steel by combining plasma nitriding (with and without white layer) and post-oxidation. *Surf. Coat. Technol.* **2020**, *385*, 125420. [[CrossRef](#)]
9. Kim, Y.-M.; Son, S.W.; Lee, W.-B. Thermodynamic and kinetic analysis of formation of compound layer during gas nitriding of AISI1018 carbon steel. *Met. Mater. Int.* **2018**, *24*, 180–186. [[CrossRef](#)]
10. Son, S.-W.; Lee, W.-B. Surface hardening and wear properties of AISI 410 martensitic stainless steel by high & low temperature gaseous nitriding. *J. Korean Inst. Surf. Eng.* **2018**, *51*, 249–255. [[CrossRef](#)]
11. Shukla, K.; Purandare, Y.P.; Khan, I.; Ehasarian, A.P.; Hovsepian, P.E.H. Effect of nitriding voltage on the impact load fatigue and fracture toughness behavior of CoCrMo alloy nitride utilising a HIPIMS discharge. *Surf. Coat. Technol.* **2020**, *400*, 126227. [[CrossRef](#)]
12. Somers, M.A.J.; Mittemeijer, E.J. Layer-growth kinetics on gaseous nitriding of pure iron: Evaluation of diffusion coefficients for nitrogen in iron nitrides. *Metall. Mater. Trans.* **1995**, *26*, 57–74. [[CrossRef](#)]
13. Conci, M.D.; Bozzi, A.C.; Franco, A.R., Jr. Effect of plasma nitriding potential on tribological behaviour of AISI D2 cold-worked tool steel. *Wear* **2014**, *317*, 188–193. [[CrossRef](#)]
14. Cho, K.T.; Song, K.; Oh, S.H.; Lee, Y.-K.; Lee, W.B. Enhanced surface hardening of AISI D2 steel by atomic attrition during ion nitriding. *Surf. Coat. Technol.* **2014**, *251*, 115–121. [[CrossRef](#)]
15. Lee, W.-B.; Yu, K.-C.; Kim, Y.-M.; Wi, J.-L. Microstructural evolution of compound layers during gaseous nitriding of AISI1045 carbon steels. *Korean J. Met. Mater.* **2016**, *54*, 475–482. [[CrossRef](#)]
16. Leite, M.V.; Figueroa, C.A.; Corujeira Gallo, S.; Rovani, A.C.; Basso, R.L.O.; Mei, P.R.; Baumvol, I.J.R.; Sinatora, A. Wear mechanisms and microstructure of pulsed plasma nitrided AISI H13 tool steel. *Wear* **2010**, *269*, 466–472. [[CrossRef](#)]
17. Gronostajski, Z.; Widomski, P.; Kaszuba, M.; Zwierzchowski, M.; Polak, S.; Piechowicz, L.; Kowalska, J.; Dlugozima, M. Influence of the phase structure of nitrides and properties of nitrided layers on the durability of tools applied in hot forging processes. *J. Manuf. Process.* **2020**, *52*, 247–262. [[CrossRef](#)]
18. Duan, Y.; Qu, S.; Jia, S.; Li, X. Evolution of the fretting wear damage of a complex phase compound layer for a nitrided high-carbon high-chromium steel. *Metals* **2020**, *10*, 1391. [[CrossRef](#)]

19. Nolan, D.; Leskovsek, V.; Jenko, M. Estimation of fracture toughness of nitride compound layers on tool steel by application of the Vickers indentation method. *Surf. Coat. Technol.* **2006**, *201*, 182–188. [[CrossRef](#)]
20. Arnaud, P.; Heripre, E.; Douit, F.; Aubin, V.; Fouvry, S.; Guiheux, R.; Branger, V.; Michel, G. Micromechanical tensile test investigation to identify elastic and toughness properties of thin nitride compound layers. *Surf. Coat. Technol.* **2021**, *421*, 127–303. [[CrossRef](#)]
21. Schwarz, B.; Gohring, H.; Meka, S.R.; Schacherl, R.E.; Mittemeijer, E.J. Pore formation upon nitriding iron and iron-based alloys: The role of alloying elements and grain boundaries. *Metall. Mater. Trans. A* **2014**, *45*, 6173–6186. [[CrossRef](#)]
22. Kovaci, H.; Yetim, A.F.; Baran, Ö.; Çelik, A. Fatigue crack growth analysis of plasma nitrided AISI 4140 low-alloy steel: Part1-constant amplitude loading. *Mater. Sci. Eng. A* **2016**, *672*, 257–264. [[CrossRef](#)]
23. Roebuck, B.; Bennett, E.; Lay, L.; Morrell, R. *Palmqvist Toughness for Hard and Brittle Materials*; Measurement Good Practice Guide, No. 9; National Physical Laboratory: Teddington, UK, 2008; pp. 9–11, 19–21.
24. Pye, D. *Practical Nitriding and Ferritic Nitrocarburizing*; ASM International: Materials Park, OH, USA, 2003; pp. 1–3, 67–68.
25. Subhash, G.; Zhang, H. Dynamic indentation response of ZrHf-based bulk metallic glasses. *J. Mater. Res.* **2007**, *22*, 478–485. [[CrossRef](#)]
26. Leroy, C.; Michel, H.; Gantois, M. Transformation of $(Cr, M)_7C_3$ -type carbides during nitriding of chromium alloyed steels. *J. Mater. Sci.* **1986**, *21*, 3467–3474. [[CrossRef](#)]
27. Van Wiggeren, P.C.; Rozendaal, H.C.F.; Mittemeijer, E.J. The nitriding behaviour of iron-chromium-carbon alloys. *J. Mater. Sci.* **1985**, *20*, 4561–4582. [[CrossRef](#)]
28. Zhao, X.; Wang, B.; Sun, D.; Li, C.; Han, L.; Gu, J. Effect of pre-existing VC carbides on nitriding and wear behavior of hot-work die steel. *Appl. Surf. Sci.* **2019**, *486*, 179–186. [[CrossRef](#)]
29. Mittermeijer, E.J.; Somers, M.A.J. *Thermochemical Surface Engineering of Steels*; Woodhead Publishing: Sawston, UK, 2015; pp. 342–343.
30. Zhang, G.; Cui, H.; Zhang, H.; Cheng, G. Micro-porous layer generated during gas nitriding and induction quenching compound treatment affects tribological properties. *Tribol. Int.* **2018**, *120*, 226–232. [[CrossRef](#)]